https://doi.org/10.5194/essd-2020-107
Preprint. Discussion started: 25 June 2020

Open Access Earth System Science Data Discussions

A 30-meter resolution dataset of China's urban impervious surface area and green space fractions, 2000–2018

Wenhui Kuang [1], Shu Zhang[1,2], Xiaoyong Li[2,3], Dengsheng Lu[4]

[1]Key Laboratory of Land Surface Pattern and Simulation, Institute of Geographic Sciences and Natural Resources Research, Chinese Academy of Sciences, Beijing 100101, China.

[2]College of Resources and Environment, University of Chinese Academy of Sciences, Beijing 10049, China.

[3]State Key Laboratory of Urban and Regional Ecology, Research Center for Eco-environmental Sciences, Chinese Academy of Sciences, Beijing 100085, China.

[4]College of Geographical Sciences, Fujian Normal University, Fuzhou 350117, China.

Correspondence to: Wenhui Kuang (kuangwh@igsnrr.ac.cn)

Abstract. Urban impervious surface area (UISA) and urban green space (UGS) are two core components of cities for characterizing urban environments. Although several global or national urban land use/cover products such as Globeland30 and FROM-GLC are available, they cannot effectively delineate the complex intra-urban land cover components. Here we proposed a new approach to map fractional UISA and UGS in China using Google Earth Engine (GEE) based on multiple data sources. The first step is to extract the vector boundaries of urban areas from China's Land Use/cover Dataset (CLUD). The UISA was retrieved using the logistic regression from the Landsat-derived annual maximum Normalized Difference Vegetation Index (NDVI). The UGS was developed through linear calibration between reference UGS from high spatial resolution image and the normalized NDVI. Thus, the China's UISA and UGS fraction datasets (CLUD-Urban) at 30-meter resolution are generated from 2000 to 2018. The overall accuracy of national urban areas is over 92%. The root mean square errors of UISA and UGS fractions are 0.10 and 0.14, respectively. The datasets indicate that total urban area of China was 7.10×10^4 km^2 in 2018, with average fractions of 70.70% for UISA and 26.54% for UGS. The UISA and UGS increased with unprecedented annual rates of 1,492.63 km^2/yr and 400.43 km^2/yr during 2000-2018. CLUD-Urban can enhance our understanding of urbanization impacts on ecological and urban dwellers' environments, and can be used in such applications as urban planning, urban environmental studies and practices. The datasets can be downloaded from https://doi.org/10.5281/zenodo.3778424 (Kuang et al., 2020).

1 Introduction

The effects of rapid urbanization on environments have been witnessed around the world (Bai et al., 2018) and profoundly contribute to the changes in biosphere, hydrosphere and atmosphere (Seto et al., 2012; J. Wu et al., 2014; Kuang et al., 2018). In China, a rapid urbanization process appeared in the 21st century (Xu and Min, 2013; Ma et al., 2014; Bai et al., 2014; Kuang, 2012; Kuang et al., 2013; Kuang et al., 2016), resulting in rapid increase in urban impervious surface area (UISA) and urban green space (UGS). This process further triggered various urban environmental problems such as urban

https://doi.org/10.5194/essd-2020-107
Preprint. Discussion started: 25 June 2020

heat island and urban flooding (Haase et al., 2014; Kuang, 2011; Kuang et al., 2015; Kuang et al., 2017; Zhang et al., 2017). Although many green areas were constructed in Chinese cities recently, China has relatively lower UGS percentage in urban areas than other developed countries such as United States (Nowak and Greenfield, 2012; Kuang et al., 2014). These urban environmental problems triggered the urgency of developing accurate urban land-cover datasets with high spatial resolution for delineating the underlying urban environments. Along with the development of earth observation technologies, remote sensing has become the mainstream method for mapping UISA and monitoring its change (Weng, 2012; Wang et al., 2013; Lu et al., 2014).

Various land-use products such as the GlobeLand30 (Chen et al., 2015), the University of Maryland (UMD) Land Cover Classification (Hansen et al., 2000), MODIS (Friedl et al., 2010), GlobCover (Bontemps et al., 2011) and FROM-GLC (Gong et al., 2013) are freely available worldwide (Grekousis et al., 2015; Dong et al., 2018). These products have different definitions of urban areas or settlements due to their different classification systems, such as the International Geosphere-Biosphere Programme (IGBP) or Food and Agriculture Organization of the United Nations (FAO) (Belward, 1996; FAO, 1997). Some urban land datasets which were constructed by supervised learning approaches were released at national or global scale with spatial resolution from 30 m to 1 km (Liu et al., 2018; He et al., 2019; Gong et al., 2019). Others such as built-up grid of the Global Human Settlement Layer (GHS Built) (Pesaresi et al., 2013) and Global Urban Footprint (GUF) (Esch et al., 2017, 2018) have been published too. Most urban land products focused on built-up land or urban area classification but cannot delineate urban land as a heterogeneous unit consisting of urban UISA, UGS and others (Chen et al., 2015). Furthermore, few urban land products provided intra-urban UISA and UGS fractions at the sub-pixel level.

Detailed UISA dataset inside a city is required as a primary urban environmental index. Numerous studies on ISA mapping at the national scale mainly rely on medium-low spatial resolution remotely sensed data such as Moderate-resolution Imaging Spectroradiometer (MODIS) and Defense Meteorological Satellite Program's Operational Linescan System (DMSP-OLS) (Gong et al., 2013; Zhou et al., 2014; Grekousis et al., 2015; Zhou et al., 2015; Kuang et al., 2016). Recently, more research is shifted to employ medium-high spatial resolution data (e.g., Landsat) to improve the products (Li et al., 2018; Liu et al., 2018; Gong et al., 2019; Gong et al., 2020; Li et al., 2020; Lin et al., 2020). The U.S. Geological Survey developed the National Land Cover Database (NLCD) and provided UISA fraction, percent tree canopy, land-cover classes and their changes with a spatial resolution of 30 m (Falcone and Homer, 2012; Yang et al., 2018). However, detailed intra-urban UISA and UGS dataset with 30 m spatial resolution for China at the national scale is not available yet, making it difficult to conduct detailed analysis of such applications as urban living environments.

In reality, the urban landscape is composed of UISA (e.g., buildings, plazas, and roads), UGS and others. Previous studies have proven that spectral mixture analysis (SMA) provides an effective tool to retrieve the UISA and UGS fraction data from Landsat multispectral imagery (Lu and Weng, 2004, 2006; Peng et al. 2016; Kuang et al., 2018). However, this method needs local knowledge for problem-specific analysis such as intra-urban land-cover analysis of a single city or a single urban agglomeration (Zhang and Weng, 2016; Xu et al., 2018). Although the globally standardized SMA can

https://doi.org/10.5194/essd-2020-107
Preprint. Discussion started: 25 June 2020

effectively extract substrate, dark and vegetation (Small, 2013), the UISA cannot be accurately and directly extracted from multispectral image without post-processing considering its widely spectral variation and different meanings between UISA and substrate (Lu et al., 2014). Because of the high correlation between UISA and vegetation indices in the urban landscape (Weng et al., 2004), fractional UISA dataset can be estimated from vegetation indices using regression-based approach (Sexton et al., 2013; Wang et al., 2017).

In this study, we developed the UISA and UGS fractions dataset with 30-m spatial resolution at national scale at five-year intervals between 2000 and 2018. This dataset provides foundation for urban dwellers' environments and enhance our understanding on the impacts of urbanization on ecological services and functions, and is also helpful in future researches and practices on urban planning and urban environmental sustainability.

2 Data sources

Landsat is the longest-running satellite series for Earth observation. Landsat Thematic Mapper (TM), Enhanced Thematic Mapper Plus (ETM+) and Operational Land Imager (OLI) data with path ranges of 118–149 and row ranges of 23–43 in China were selected (Table 1). Because of the cloud problem, we extended image acquisition dates within three years. Since available images around 2010 were relatively low, we selected China-Brazil Earth Resources Satellite (CBERS-1) and Huan Jing (HJ-1A/B) satellite images with similar spectral and spatial resolutions as supplements for data analysis.

3. Mapping urban boundaries

The Chinese Academy of Sciences has updated China's national CLUD every five years since 2000 (Liu, Liu, Tian et al., 2005; Liu, Liu, Zhuang et al., 2005; Liu et al., 2010), forming a time series of land-use/cover products at a spatial resolution of 30 m. This product provides six first-level classes – cropland, woodland, grassland, water body, built-up area and unused land. The built-up area was divided into three second-level classes – urban land, rural area, and industrial and mining land beyond cities. We extracted the vector boundaries of urban land from the CLUD's dataset (Kuang et al., 2016). In this classification system, urban area is referred to as large, medium and small cities where the construction land is located in counties and towns. However, this dataset regards a city as a homogeneous unit, thus does not reflect intra land-cover status, i.e., UISA, UGS, and others.

The underlying urban condition shows highly spatial heterogeneity (Kuang et al., 2017), which is mosaicked with UISA, UGS and others. We proposed a hierarchical-based urban land-cover classification approach, which divided urban landscapes into UISA, UGS, and others. UISA refers to the urban impervious surface features caused by artificial land-use activities, like building roofs, asphalt or cement roads, and parking lots. UGS is an important component of the green infrastructure of cities and provides a range of ecosystem services, as well as cultural services such as recreation and restoration, including parks, trees and grass. UGS provides positive influences on urban environments, but most urban classification products tend to exclude this component (Hamdi and Schayes, 2008).

https://doi.org/10.5194/essd-2020-107
Preprint. Discussion started: 25 June 2020

Open Access Earth System Science Data Discussions

Urban areas as a composite of UISA and UGS have different spectral characteristics in Landsat imagery, as shown in Fig. 1 as an example for a comparison of old cities and new cities in Suzhou. Because buildings in the old city are distributed compactly, their colours in Landsat images are relatively dark, while the new city is dominated by industrial lands with well-designed urban landscapes, their colours appear bright. With prior knowledge of image classification and human-computer visual interpretation, we extracted China's urban land by detecting the city's boundaries from CLUD: the interpretation symbols of cities in Landsat images were firstly established (Fig. 1), the polygons in GIS were then used to delineate urban boundaries, and were created and labelled as urban area.

4 Retrieval of UISA and UGS fractions

4.1 Retrieval of UISA fraction

The UISA and UGS were characterized as percentage of UISA or UGS in a pixel. In arid and semiarid regions, however, percentage of vegetation cover is seasonally dependent (Lu et al., 2008), therefore, we used multitemporal normalized difference vegetation index (NDVI) data in a year to generate an annual NDVI maximum image to improve the accuracy of vegetation characterization. As a negative correlation between NDVI and UISA fraction was found at the pixel level (Kuang et al., 2016), a regression model based on the relationship between NDVI and UISA fraction was established to estimate UISA fraction.

According to the statistical results, the negative correlation between UISA fraction and NDVI value does not fit well in a linear regression relationship. Under the linear assumption, UISA fraction is overestimated in the low-value range and underestimated in the high-value range (Zhang et al., 2009). However, we found that the logistic regression model (LRM) can reduce the shortcomings of the linear regression model mentioned above, thus, LRM was selected for UISA fraction estimation (Walker and Duncan, 1967). In addition, the input parameters required by logistic regression—UISA classification data with binary value and NDVI maximum data—can be obtained from existing datasets. The major steps include (1) the annual NDVI maximum value and UISA classification data were retrieved from Landsat images, (2) the parameters of the logistic regression model were estimated, and (3) the annual NDVI maximum value was used as input data to estimate the UISA fraction at the pixel level using the developed LRM, which can be expressed as:

$$\mathrm{P}(t) = \frac{1}{1+e^{t}} \tag{1}$$

$$t = a \times (1 - NDVI_{max}) + b \tag{2}$$

where a and b represent the parameters of LRM; $NDVI_{max}$ is the annual NDVI maximum value:

$$NDVI_{max} = \max(NDVI_1, NDVI_2, \cdots, NDVI_i) \tag{3}$$

where $NDVI_i$ is the NDVI value of the i^{th} image. Individual NDVI was calculated from Landsat image and all images were collected in Google Earth Engine (GEE) (Gorelick et al., 2017). In this study, all Landsat 5/7 images in 2000, 2005 and 2010 and all Landsat 8 images in 2015 and 2018 were selected to calculate the NDVI maximum value in a given year.

https://doi.org/10.5194/essd-2020-107
Preprint. Discussion started: 25 June 2020


Open Access Earth System Science Data Discussions

Huge discrepancies in the UISA and UGS components of different cities were found because of different climate and geographical conditions. The UISA is often related to urban economic and geographic conditions, and the same economic region can be assumed to have similar UISA density. According to the Chinese economic and geographic zones, we selected 28 typical cities to calibrate UISA data using the LRM model. For each city, 1,000 samples for UISA and UGS were randomly selected. They were used as the input for LRM to calibrate parameters (Fig. 2, Fig. 3). The average value of the parameters in each economic and geographic zone is obtained as a regression parameter for all cities in the same zone (Table 2).

4.2 Retrieval of UGS fraction

According to sample plots collected from typical cities based on Chinese economic and geographic zones, the UGS were calibrated from the vegetation cover in urban landscapes with the following equations:

$$VC = \frac{NDVI - NDVI_{soil}}{NDVI_{veg} - NDVI_{soil}}, \quad (4)$$

$$UGS = \alpha + \beta VC, \quad (5)$$

Where VC is the vegetation cover in the urban landscape. $NDVI_{veg}$ and $NDVI_{soil}$ are NDVI values (the annual NDVI maximum image, see equation (3)) at pure vegetation and pure bare soils. α and β are constant and slope in the linear regression.

5 Validation of CLUDs and of UISA and UGS fractions

The unified quality check and data integration were performed for the years of 2000, 2005, 2010, 2015 and 2018 to ensure the quality and consistency of the interpretation results. In the process of land-use/cover interpretation, field investigations were mainly carried out in autumn in the northern part of the country and in spring in the southern part. High spatial resolution images from Google Earth were used for validation (Liu et al., 2014; Zhang et al., 2014; Kuang et al., 2016; Ning et al., 2019). At least 2,200 points for each interval were randomly generated throughout China. Based on validation results, the overall accuracy of urban land or built-up area was 92–99% for each given year (Table 3) and the overall accuracy for urban land change was 95–97% for each period (Table 4).

https://doi.org/10.5194/essd-2020-107
Preprint. Discussion started: 25 June 2020

Google Earth images with higher spatial resolution than Landsat images were employed for the validation of UISA and UGS fractions. Firstly, the 30 m × 30 m UISAs were rectified with Google Earth images. A total of 1,111 validation samples with a window size of 3 × 3 pixels (90 m × 90 m grids) for each sample plot were randomly acquired from 44 cities in different regions in China for validation (Fig. 4). Mean UISA and UGS densities in each grid were calculated. The actual value in the same area was obtained by visual interpretation from Google Earth images. Accuracy assessment of UISA and UGS was performed by root mean square error (RMSE) and correlation coefficient (R). The validation of UISA and UGS fractions in each period shows that the RMSEs were 0.09–0.12 and 0.12–0.17 respectively,, and the R values were 0.89–0.93 and 0.85–0.89 respectively (Table 3). For the validation for change detection results at different period, we chose 741 samples (90m×90m) within urban area for validation. We used medium relatively error (MRE) and R to examine the accuracy. The MRE values of UISA and UGS fractions for each period were 5.2–6.8% and 5.9–7.1% respectively (Table 4).

6 Results

We compared the vector boundaries of urban areas with the existing land-use products and found their obvious discrepancies because of the differences in data production, data source, resolution and definition of urban land-use types. The spatial resolutions of land-cover products range from 30 m to 1000 m, and their classification systems are based on IGBP or FAO frameworks (Belward, 1996; FAO, 1997). Figure 5 provides a comparison of a list of urban land datasets (see Table 5 for these datasets), showing that our product has better performance in delineating the detailed intra-urban land cover spatial patterns note: both of the GHS Built and GlobaLand 30 products only have two years). The intra-urban land-cover is more complex than rural area. However, most urban land products cannot effectively distinguish urban and rural land using an automatic classification method (Fig. 5b, c, d, e). In our dataset, urban area is emphasized from the area where county's or town's government located, usually with a sufficient size of population. Because other products cannot effectively distinguish urban and rural lands, their urban areas were overestimated considerably (Fig. 5). CLUD-Urban can delineate intra-urban land-cover at pixel level, providing more elaborate than other products.

China's UISA shows an increasing trend, from 2.22×10^4 km^2 in 2000 to 5.20×10^4 km^2 in 2018 (Fig. 6), similar to the urban expansion rates. From the perspective of the quality of dwellers' environments, the UISA was 68.34%-71.57% in 2000-2018, showing a higher UISA density in China's urban area than other developed countries, like the USA (Kuang et al., 2014). As shown in Fig. 6, the UISA across China is mainly clustered in the coastal and the central regions and relatively discrete in the western region. The pattern of "high in east and low in west" remained unchanged during the period of 2000 and 2018. Similar to the trend of urban land area and UISA, China's UGS shows an increasing trend. The total UGS increased from 1.00×10^4 km^2 in 2000 to 1.83×10^4 km^2 in 2018 (Fig. 7). Looking at both UISA and UGS in urban areas, our results indicate a slight decrease in UGS density and increase in UISA density. The UGS was 30.77%, 29.86%, 30.31%, 27.70% and 26.04%, in 2000, 2005, 2010, 2015 and 2018, respectively. As shown in Fig. 7, UGS is mainly distributed in coastal, northeastern, and southwestern China. The largest increase occurred in the coastal and northeastern regions.

https://doi.org/10.5194/essd-2020-107
Preprint. Discussion started: 25 June 2020

To illustrate the pattern of national urban land change, we analysed the process of urban expansion since 2000, together with UISA and UGS dynamics (Fig. 6, Fig. 7 and Fig. 8). The growths of UISA and UGS were obvious in main urban areas, like Beijing-Tianjin, Yangtze River Delta and Guangdong–Hong Kong–Macao Great Bay Area. Both UISA and UGS showed an increasing trend associated with urban expansion. High proportions of UISA and UGS were located in eastern China because of its good economic conditions. High proportional UISA represents buildings, roads and plazas, whereas low proportional UISA represents parks and greenbelts with ecological functions. This dataset can characterize differences among the selected cities. Some cities, like Beijing and Nanjing with well-planned urban landscapes had relatively small proportions of UISA (59.35% and 68.19%, respectively) and high proportions of UGS (38.61% and 30.33%, respectively) in their urban landscapes in 2018.

7 Data availability

All data presented in this paper are available in https://doi.org/10.5281/zenodo.3778424 (Kuang et al., 2020). This dataset covers five years (i.e., 2000, 2005, 2010 2015 and 2018) with a spatial resolution of 30 m. Detailed metadata description is provided, including contact information.

8 Conclusion

The CLUD-Urban – China's UISA and UGS fraction datasets with 30-m spatial resolution was generated using multiple data sources. CLUD-Urban provided detailed delineation in UISA and UGS components for 2000, 2005, 2010, 2015 and 2018 in China. The novelty of this dataset, comparing to other products, is that it takes cities as heterogeneous units at the pixel level, which is consisted of UISA, UGS, and others. The accuracy of the CLUD-Urban dataset is 91.98% using the integrated approach of visual interpretation and prior knowledge. The RMSEs of UISA and UGS fractions are 0.10 and 0.14, respectively. Results from the analysis of urban areas, including UISA and UGS, show large regional differences in China. CLUD-Urban provides fundamental data sources for examining urban environment issues and for delineating intra-urban structure or urban landscape at the national scale.

Author contribution

KW, ZS and LX designed the research; ZS and LX implemented the research; KW, ZS and LD wrote the paper.

Competing interests

The authors declare no conflict of interest.

https://doi.org/10.5194/essd-2020-107
Preprint. Discussion started: 25 June 2020

Open Access Earth System Science Data Discussions

Acknowledgments

This study was supported by National Natural Science Foundation of China (NSFC) (41871343) and Strategic Priority Research Program A of the Chinese Academy of Sciences (XDA23100201). We thank Dr. Fengyun Sun and Dr. Rafiq Hamdi for their help in manuscript editing.

References

As-syakur, A. R., Adnyana, I. W. S., Arthana, I. W., Nuarsa, I. W. Enhanced built-up and bareness index (EBBI) for mapping built-up and bare land in an urban area. Remote Sens., 4(10), 2957-2970, https://doi.org/10.3390/rs4102957, 2012.

Bai, X., Shi, P., and Liu, Y.: Society: realizing China's urban dream, Nature, 509, 158–160, https://doi.org/10.1038/509158a, 2014.

Bai, X., Dawson, R.J., Urge-Vorsatz, D., Delgado, G.C., Barau, A.S., Dhakal, S., Dodman, D., Leonardsen, L., Masson-Delmotte, V., Roberts, D., and Schultz, S. Six research priorities for cities and climate change. Nature, 555: 19-21. https://doi.org/10.1038/d41586-018-02409-z. 2018.

Belward A. (Ed.): The IGBP-DIS global 1 km land cover data set "DISCover": proposal and implementation plans. Report of the Land Cover Working Group of the IGBP-DIS. IGBP-DIS Working Paper, No. 13. Stockholm, 1996.

Bontemps, S., P. Defourny, E. Bogaert, O. Arino, V. Kalogirou, and J. Perez. Globcover 2009. Products Description and Validation Reports, available at: https://epic.awi.de/31014/16/GLOBCOVER2009_Validation_Report_2-2.pdf. (last access: April 18, 2019), 2011.

Chen, J., Chen, J., Liao, A., Cao, X., Chen, L., Chen, X., He, C., Han, G., Peng, S., Lu, M., Zhang, W., Tong, X., and Mills, J.: Global land cover mapping at 30 m resolution: a POK-based operational approach, ISPRS J. Photogramm., 103, 7–27, https://doi.org/10.1016/j.isprsjprs.2014.09.002, 2015.

Dong, J., Kuang, W., and Liu, J.: Continuous land cover change monitoring in the remote sensing big data era, Science China Earth Sciences, 60, 2223–2224, https://doi.org/10.1007/s11430-017-9143-3, 2017.

Dong, J., Kuang, W., Liu, J. Continuous land cover change monitoring in the remote sensing big data era, Science China Earth Sciences, 60, 2223-2224, https://doi.org/10.1007/s11430-017-9143-3, 2017.

Esch T., Bachofer F., Heldens W., Hirner A., Marconcini M., Palacios-Lopez D., Roth A., Üreyen S., Zeidler J., Dech S. and Gorelick N.: Where we live—a summary of the achievements and planned evolution of the global urban footprint, Remote Sens., 10, 895, https://doi.org/10.3390/rs10060895, 2018.

Esch T., Heldens W., Hirner A., Keil M., Marconcini M., Roth A., Zeidler J., Dech S. and Strano E.: Breaking new ground in mapping human settlements from space – the Global Urban Footprint, Isprs J. Photogramm., 134, 30-42, https://doi.org/10.1016/j.isprsjprs.2017.10.012, 2017.

https://doi.org/10.5194/essd-2020-107
Preprint. Discussion started: 25 June 2020

Falcone, J. A., and Homer, C. G.: Generation of a U.S. national urban land-use product, Photogramm. Eng. Rem. S., 78, 1057–1068, https://doi.org/10.14358/PERS.78.10.1057, 2012.

FAO (Food and Agriculture Organization of the United Nations). Africover land cover classification, Rome, 1997.

Friedl, M. A., Sulla-Menashe, D., Tan, B., Schneider, A., Ramankutty, N., Sibley, A., and Huang, X.: MODIS Collection 5 global land cover: algorithm refinements and characterization of new datasets, Remote Sens. Environ., 114, 168–182, https://doi.org/10.1016/j.rse.2009.08.016, 2010.

Gong P., Li X. and Zhang W.: 40-Year (1978–2017) human settlement changes in China reflected by impervious surfaces from satellite remote sensing, Sci. Bull., 64, 756-63, https://doi.org/10.1016/j.scib.2019.04.024, 2019.

Gong, P., Wang, J., Yu, L., Zhao, Y., Zhao, Y., Liang, L., Niu, Z., Huang, X., Fu, H., Liu, S., Li, C., Li, X., Fu, W., Liu, C., Xu, Y., Wang, X., Cheng, Q., Hu, L., Yao, W., Zhang, H., Zhu, P., Zhao, Z., Zhang, H., Zheng, Y., Ji, L., Zhang, Y., Chen, H., Yan, A., Guo, J., Yu, L., Wang, L., Liu, X., Shi, T., Zhu, M., Chen, Y., Yang, G., Tang, P., Xu, B., Giri, C., Clinton, N., Zhu, Z., Chen, J., and Chen, J.: Finer resolution observation and monitoring of global land cover: first mapping results with Landsat TM and ETM+ data, Int. J. Remote Sens., 34, 2607–2654, https://doi.org/10.1080/01431161.2012.748992, 2013.

Gong, P., Li, X., Wang, J., Bai, Y., Chen, B., Hu, T., Liu, X., Xu, B., Yang, J., Zhang, W. and Zhou, Y.: Annual maps of global artificial impervious area (GAIA) between 1985 and 2018, Remote Sens. Environ., 236, 111510, https://doi.org/10.1016/j.rse.2019.111510, 2020.

Gorelick, N., Hancher, M., Dixon, M., Ilyushchenko, S., Thau, D., and Moore, R.: Google Earth Engine: planetary-scale geospatial analysis for everyone, Remote Sens. Environ., 202, 18–27, https://doi.org/10.1016/j.rse.2017.06.031, 2017.

Grekousis, G., Mountrakis, G., and Kavouras, M.: An overview of 21 global and 43 regional land-cover mapping products, Int. J. Remote Sens., 36, 5309–5335, https://doi.org/10.1080/01431161.2015.1093195, 2015.

Haase, D., Larondelle, N., Andersson, E., Artmann, M., Borgström, S., Breuste, J., Gomez-Baggethun, E., Gren, Å., Hamstead, Z., Hansen, R., Kabisch, N., Kremer, P., Langemeyer, J., Rall, E. L., McPhearson, T., Pauleit, S., Qureshi, S., Schwarz, N., Voigt, A., Wurster, D., and Elmqvist, T.: A quantitative review of urban ecosystem service assessments: concepts, models, and implementation, Ambio, 43, 413–433, https://doi.org/10.1007/s13280-014-0504-0, 2014.

Hamdi, R., Schayes, G., Sensitivity study of the urban heat island intensity to urban characteristics, Int. J. Climatol., 28, 973-982, https:// doi.org/10.1002/joc.1598, 2007.

Hansen, M. C., Defries, R. S., Townshend, J. R. G., and Sohlberg, R.: Global land cover classification at 1 km spatial resolution using a classification tree approach, Int. J. Remote Sens., 21, 1331–1364, https://doi.org/10.1080/014311600210209, 2000.

He C., Liu Z., Gou S., Zhang Q., Zhang J. and Xu L.: Detecting global urban expansion over the last three decades using a fully convolutional network, Environ. Res. Lett., 14, 34008, https://doi.org/10.1088/1748-9326/aaf936, 2019.

Kuang, W.: Simulating dynamic urban expansion at regional scale in Beijing-Tianjin-Tangshan Metropolitan Area, J. Geogr. Sci., 21, 317–330, https://doi.org/10.1007/s11442-011-0847-4, 2011.

https://doi.org/10.5194/essd-2020-107
Preprint. Discussion started: 25 June 2020

Kuang, W.: Evaluating impervious surface growth and its impacts on water environment in Beijing-Tianjin-Tangshan metropolitan area, J. Geogr. Sci., 22, 535–547, https://doi.org/10.1007/s11442-012-0945-y, 2012.

Kuang, W., Liu, J., Zhang, Z., Lu, D., and Xiang, B.: Spatiotemporal dynamics of impervious surface areas across China during the early 21st century, Chin. Sci. Bull., 58, 1691–1701, https://doi.org/10.1007/s11434-012-5568-2, 2013.

Kuang, W., Chi, W., Lu, D., and Dou, Y.: A comparative analysis of megacity expansions in China and the U.S.: patterns, rates and driving forces, Landscape Urban Plan., 132, 121–135, https://doi.org/10.1016/j.landurbplan.2014.08.015, 2014.

Kuang, W., Dou, Y., Zhang, C., Chi, W., Liu, A., Liu, Y., Zhang, R., and Liu, J.: Quantifying the heat flux regulation of metropolitan land use/land cover components by coupling remote sensing modeling with in situ measurement, J. Geophys. Res.-Atmos., 120, 113–130, https://doi.org/10.1002/2014JD022249, 2015.

Kuang, W., Liu, J., Dong, J., Chi, W., and Zhang, C.: The rapid and massive urban and industrial land expansions in China between 1990 and 2010: a CLUD-based analysis of their trajectories, patterns, and drivers, Landscape Urban Plan., 145, 21–33, https://doi.org/10.1016/j.landurbplan.2015.10.001, 2016.

Kuang, W., Yang, T., Liu, A., Zhang, C., Lu, D., and Chi, W.: An EcoCity model for regulating urban land cover structure and thermal environment: taking Beijing as an example, Sci. China Ser. D-Earth Sci., 60, 1098–1109, https://doi.org/10.1007/s11430-016-9032-9, 2017.

Kuang, W., Yang, T., Yan, F.: Examining urban land-cover characteristics and ecological regulation during the construction of Xiong'an New District, Hebei Province, China, J. Geogr. Sci, 28, 109-123, https://doi.org/10.1007/s11442-018-1462-4, 2018.

Kuang, W., Zhang, S., Li, X., Lu, D.: A 30-meter resolution dataset of impervious surface area and green space fractions of China's cities, 2000-2018, Zenodo, https://doi.org/10.5281/zenodo.3778424, 2020.

Li, H., Wang, C., Zhong, C., Su, A., Xiong, C., Wang, J., Liu, J.: Mapping urban bare land automatically from Landsat imagery with a simple index. Remote Sens., 9(3), 249, https://doi.org/10.3390/rs9030249, 2019.

Li, X., Zhou, Y., Zhu, Z., Liang, L., Yu, B. and Cao W.: Mapping annual urban dynamics (1985–2015) using time series of Landsat data. Remote Sens. Environ., 216, 674-683, https://doi.org/10.1016/j.rse.2018.07.030, 2018.

Li, X., Zhou, Y., Zhu, Z. and Cao W.: A national dataset of 30 m annual urban extent dynamics (1985-2015) in the conterminous United States. Earth Syst. Sci. Data, 12(1), https://doi.org/10.5194/essd-12-357-2020, 2020.

Lin, Y., Zhang, H., Lin, H., Gamba, P. E., Liu, X.: Incorporating synthetic aperture radar and optical images to investigate the annual dynamics of anthropogenic impervious surface at large scale. Remote Sens. Environ., 242, 111757, https://doi.org/10.1016/j.rse.2020.111757, 2020.

Liu, J., Liu, M., Tian, H., Zhuang, D., Zhang, Z., Zhang, W., Tang, X., and Deng, X.: Spatial and temporal patterns of China's cropland during 1990–2000: an analysis based on Landsat TM data, Remote Sens. Environ., 98, 442–456, https://doi.org/10.1016/j.rse.2005.08.012, 2005.

https://doi.org/10.5194/essd-2020-107
Preprint. Discussion started: 25 June 2020

Liu, J., Liu, M., Zhuang, D., Zhang, Z., Deng, X.: Study on spatial pattern of land-use change in China during 1995–2000, Sci. China Ser. D-Earth Sci., 46, 3732003, 2005.

Liu, J., Zhang, Z., Xu, X., Kuang, W., Zhou, W., Zhang, S., Li, R., Yan, C., Yu, D., Wu, S., and Jiang, N.: Spatial patterns and driving forces of land use change in China during the early 21st century, J. Geogr. Sci., 20, 483–494, https://doi.org/10.1007/s11442-010-0483-4, 2010.

Liu, J., Kuang, W., Zhang, Z., Xu, X., Qin, Y., Ning, J., Zhou, W., Zhang, S., Li, R., Yan, C., Wu, S., Shi, X., Jiang, N., Yu, D., Pan, X., and Chi, W.: Spatiotemporal characteristics, patterns, and causes of land-use changes in China since the late 1980s, J. Geogr. Sci., 24, 195–210, https://doi.org/10.1007/s11442-014-1082-6, 2014.

Liu X., Hu G., Chen Y., Li X., Xu X., Li S., Pei F., Wang S.: High-resolution multi-temporal mapping of global urban land using Landsat images based on the Google Earth Engine Platform, Remote Sens. Environ., 209, 227-39, https://doi.org/10.1016/j.rse.2018.02.055, 2018.

Lu, D., and Weng, Q.: Spectral mixture analysis of the urban landscape in Indianapolis with Landsat ETM plus imagery, Photogramm. Eng. Rem. S., 70, 1053–1062, https://doi.org/10.14358/PERS.70.9.1053, 2004.

Lu, D., and Weng, Q.: Use of impervious surface in urban land-use classification, Remote Sens. Environ., 102, 146–160, https://doi.org/10.1016/j.rse.2006.02.010, 2006.

Lu, D., Tian, H., Zhou, G., Ge, H.: Regional mapping of human settlements in southeastern China with multisensor remotely sensed data, Remote Sens. Environ., 112, 3668–3679, https://doi.org/10.1016/j.rse.2008.05.009, 2008.

Lu, D., Li, G., Kuang, W., and Moran, E.: Methods to extract impervious surface areas from satellite images, Int. J. Digit. Earth, 7, 93–112, https://doi.org/10.1080/17538947.2013.866173, 2014.

Lu D., Li L., Li G., Fan P., Ouyang Z., Moran E.: Examining spatial patterns of urban distribution and impacts of physical conditions on urbanization in coastal and inland metropoles, Remote Sens., 10, 1101, https://doi.org/10.3390/rs10071101, 2018.

Ma, Q., He, C., Wu, J., Liu, Z., Zhang, Q., and Sun, Z.: Quantifying spatiotemporal patterns of urban impervious surfaces in China: an improved assessment using nighttime light data, Landscape Urban Plan., 130, 36–49, https://doi.org/10.1016/j.landurbplan.2014.06.009, 2014.

Ning J., Liu J., Kuang W., Xu X., Zhang S., Yan C., Li R., Wu S., Hu Y., Du G., Chi W., Pan T., Ning J.: Spatiotemporal patterns and characteristics of land-use change in China during 2010–2015, J. Geogr. Sci., 28, 547-62, https://doi.org/10.1007/s11442-018-1490-0, 2018.

Nowak, D.J., and Greenfield, E.J.: Tree and impervious cover in the United States, Landscape Urban Plan., 107, 21–30, https://doi.org/10.1016/j.landurbplan.2012.04.005, 2012.

Pesaresi M., Huadong G., Blaes X., Ehrlich D., Ferri S., Gueguen L., Halkia M., Kauffmann M., Kemper T., Lu L., Marin-Herrera M. A., Ouzounis G. K., Scavazzon M., Soille P., Syrris V. and Zanchetta L.: A Global Human Settlement Layer from optical hr/vhrrs data: concept and first results, Ieee J-Stars., 6, 2102-31, https://doi.org/10.1109/JSTARS.2013.2271445, 2013.

https://doi.org/10.5194/essd-2020-107
Preprint. Discussion started: 25 June 2020

Peng, J., Shen, H., Wu, W., Liu, Y., and Wang, Y.: Net primary productivity (NPP) dynamics and associated urbanization driving forces in metropolitan areas: a case study in Beijing City, China, Landscape Ecol., 31, 1077–1092, https://doi.org/10.1007/s10980-015-0319-9, 2016.

Sexton J. O., Song X., Huang C., Channan S., Baker M. E. and Townshend J. R.: Urban growth of the Washington, D.C.–Baltimore, MD metropolitan region from 1984 to 2010 by annual, Landsat-based estimates of impervious cover, Remote Sens. Environ., 129, 42-53, https://doi.org/10.1016/j.rse.2012.10.025, 2013.

Seto, K. C., Guneralp, B., and Hutyra, L. R.: Global forecasts of urban expansion to 2030 and direct impacts on biodiversity and carbon pools, P. Nat. Acad. Sci. USA, 109, 16083–16088, https://doi.org/10.1073/pnas.1211658109, 2012.

Small C. and Milesi C.: Multi-scale standardized spectral mixture models, Remote Sens. Environ., 136, 442-54, https://doi.org/10.1016/j.rse.2013.05.024, 2013.

Walker, S. H.; and Duncan, D. B.: Estimation of the probability of an event as a function of several independent variables, Biometrika, 54 (1/2), 167–178, https://10.2307/2333860, 1967.

Wang, H., Lu, S., Wu, B., and Li, X.: Advances in remote sensing of impervious surfaces extraction and its applications, Advance in Earth Sciences, 28, 327–336, 2013.

Wang, P., Huang, C., Brown de Colstoun, E. C., Tilton, J. C., and Tan, B.: Global Human Built-up And Settlement Extent (HBASE) dataset from Landsat, NASA Socioeconomic Data and Applications Center (SEDAC), Palisades, NY, https://doi.org/10.7927/H4DN434S, 2017.

Weng, Q.: Remote sensing of impervious surfaces in the urban areas: requirements, methods, and trends, Remote Sens. Environ., 117, 34–49, https://doi.org/10.1016/j.rse.2011.02.030, 2012.

Weng, Q., Lu, D., and Schubring, J.: Estimation of land surface temperature–vegetation abundance relationship for urban heat island studies. Remote Sensing of Environment, 89(4), 467–483, https://doi.org/10.1016/j.rse.2003.11.005. 2004.

Wu, C., and Murray, A. T.: Estimating impervious surface distribution by spectral mixture analysis, Remote Sens. Environ., 84, 493–505, https://doi.org/10.1016/S0034-4257(02)00136-0, 2003.

Wu, J., Xiang, W., and Zhao, J.: Urban ecology in China: historical developments and future directions, Landscape Urban Plan., 125, 222–233, https://doi.org/10.1016/j.landurbplan.2014.02.010, 2014.

Xu, H.: Modification of normalised difference water index (NDWI) to enhance open water features in remotely sensed imagery, Int. J. Remote Sens., 27, 3025–3033, https://doi.org/10.1080/01431160600589179, 2006.

Xu, J., Zhao, Y., Zhong, K., Zhang, F., Liu, X., and Sun, C.: Measuring spatio-temporal dynamics of impervious surface in Guangzhou, China, from 1988 to 2015, using time-series Landsat imagery, Sci. Total Environ., 627, 264–281, https://doi.org/10.1016/j.scitotenv.2018.01.155, 2018.

Xu, X., and Min, X.: Quantifying spatiotemporal patterns of urban expansion in China using remote sensing data, Cities, 35, 104–113, https://doi.org/10.1016/j.cities.2013.05.002, 2013.

Yang L., Jin S., Danielson P., Homer C., Gass L., Bender S. M., Case A., Costello C., Dewitz J., Fry J., Funk M., Granneman B., Liknes G. C., Rigge M. and Xian G.: A new generation of the United States National Land Cover

https://doi.org/10.5194/essd-2020-107
Preprint. Discussion started: 25 June 2020

Database: Requirements, research priorities, design, and implementation strategies, Isprs J. Photogramm., 146, 108-23, https://doi.org/10.1016/j.isprsjprs.2018.09.006, 2018.

Zhang, L., and Weng, Q.: Annual dynamics of impervious surface in the Pearl River delta, China, from 1988 to 2013, using time series Landsat imagery, ISPRS J. Photogramm., 113, 86–96, https://doi.org/10.1016/j.isprsjprs.2016.01.003, 2016.

Zhang, Z., Wang, X., Zhao, X., Liu, B., Liu, F., Yi, L., Zuo, L., Wen, Q., Xu, J., and Hu, S.: A 2010 update of National Land Use/Cover Database of China at 1:100000 scale using medium spatial resolution satellite images, Remote Sens. Environ., 149, 142–154, https://doi.org/10.1016/j.rse.2014.04.004, 2014.

Zhang, Z., Wang, W., Cheng, M., Liu, S., Xu, J., He, Y., and Meng, F.: The contribution of residential coal combustion to PM 2.5 pollution over China's Beijing-Tianjin-Hebei region in winter, Atmos. Environ., 159, 147–161, https://doi.org/10.1016/j.atmosenv.2017.03.054, 2017.

Zhang, C., Kuang, W., Wu, J., Liu, J. and Tian, H.: Industrial land expansion in rural China threatens food and environmental securities, Front. Env. Sci. Eng., in review, 2020.

Zhang, Y., Odeh, I. O. A., Han, C.: Bi-temporal characterization of land surface temperature in relation to impervious surface area, NDVI and NDBI, using a sub-pixel image analysis, Int. J. Appl. Earth. Obs., 11, 256–264, https://doi.org/10.1016/j.jag.2009.03.001, 2009.

Zhou, Y., Smith, J. S., Elvidge, C. D., Zhao, K., Thomson, A., M. and Imhoff, L. M.: A cluster-based method to map urban area from DMSP/OLS nightlights, Remote Sens. Environ., 147, 173–185, https://doi.org/10.1016/j.rse.2014.03.004, 2014.

Zhou, Y., Smith, J. S., Zhao, K., Imhoff, L. M., Thomson, A. M., Bondlamberty, B., Asrar, G., Zhang, X., He, C. and Elvidge, C. D.: A global map of urban extent from nightlights, Environ. Res. Lett., 10(5), 054011, https://doi.org/10.1088/1748-9326/10/5/054011, 2015.

https://doi.org/10.5194/essd-2020-107
Preprint. Discussion started: 25 June 2020

Open Access Earth System Science Data Discussions

Table 1: The multitemporal data series used in this research

Year	Path	Row	Image period	Sensor	Spatial resolution (m)
2000			1999–2001	TM, ETM+	30
2005			2004–2006	TM	30
2010	118–149	23–43	2009–2011	TM, HJ-1, CBERS -1	30
2015			2014–2016	OLI	30
2018			2017-2019	OLI	30

Note: TM, Landsat Thematic Mapper; ETM+, Landsat Enhanced Thematic Mapper Plus; HJ, Huan Jing; CBERS, China Brazil Earth Resources Satellite; OLI, Landsat 8 Operational Land Imager.

400

Table 2: Parameters of the logistic regression models based on selected cities in China.

City	a	b	Score
Changsha	0.013	-6.353	0.866
Hefei	0.011	-6.148	0.855
Taiyuan	0.014	-7.974	0.873
Wuhan	0.008	-4.425	0.802
Central region	0.012	-6.225	0.849
Tianjin	0.007	-3.946	0.780
Haikou	0.012	-6.357	0.897
Jinan	0.015	-9.149	0.879
Hangzhou	0.010	-5.032	0.887
Nanjing	0.006	-3.503	0.768
Shenzhen	0.011	-5.891	0.873
Qingdao	0.013	-8.399	0.845
Xiamen	0.009	-5.224	0.833
Ningbo	0.010	-4.988	0.862
Foshan	0.007	-3.957	0.757
Dongguan	0.006	-3.904	0.792
Beijing	0.010	-5.311	0.876
Chengdu	0.012	-6.669	0.834
Shanghai	0.008	-4.362	0.784
Coastal region	0.010	-5.478	0.833
Changchun	0.013	-6.054	0.893
Harbin	0.012	-5.569	0.939
Shenyang	0.011	-5.370	0.848
Dalian	0.012	-7.240	0.881
Northeastern region	0.012	-6.058	0.890
Guiyang	0.014	-7.902	0.884
Kunming	0.013	-7.074	0.878
Nanning	0.015	-0.722	0.913

https://doi.org/10.5194/essd-2020-107
Preprint. Discussion started: 25 June 2020

City	a	b	Score
Xian	0.014	-7.571	0.911
Lanzhou	0.017	-12.357	0.827
Urumqi	0.003	-2.058	0.686
Western region	0.013	-6.281	0.850

Note: a, b are parameters of LRM

Table 3: Accuracy assessments for the extracted urban land and UISA, UGS fractions.

Year	Urban land	UISA		UGS	
	Overall accuracy	RMSE	R	RMSE	R
2000	98.92%	0.12	0.89	0.17	0.85
2005	97.01%	0.11	0.89	0.17	0.87
2010	93.99%	0.10	0.91	0.16	0.87
2015	91.98%	0.09	0.93	0.12	0.89
2018	95.49%	0.10	0.91	0.17	0.87

Note: The validations of urban land were obtained from Zhang et al. (2014) and Ning et al. (2019)

405

Table 4: Accuracy assessments for urban land and UISA, UGS changes.

Period	Overall accuracy of urban land	MRE of UISA	MRE of UGS
2000-2005	97.01%	5.69%	7.09%
2005-2010	95.93%	5.33%	5.86%
2010-2015	94.99%	6.83%	6.68%
2015-2018	95.23%	5.21%	5.98%

MRE, medium relatively error

Table 5: A summary of existing urban land products.

Name	Spatial resolution	Abbreviation	Method	Reference
Chinese Urban Land use/cover Dataset	30m	CLUD-Urban	Visual interpretation and machine learning	-
Land Cover from Moderate-resolution Imaging Spectroradiometer	500m	MODIS LC	Decision tree classification	(Friedl et al., 2010)
European Space Agency global land-cover data	300m	ESA LC	Unsupervised classification and change detection	(Bontemps et al., 2011)
Built-up grid of the Global Human Settlement Layer	30m	GHS Built	Symbolic machine learning	(Pesaresi et al., 2013)
Global Land Cover at 30m resolution	30m	GlobaLand30	Pixel-Object Knowledge (POK)-based classification	(Chen et al., 2015)
Multi-temporal Global Impervious Surface	30m	MGIS	Normalized urban areas composite index	(Liu et al., 2018)
Annual maps of global artificial impervious area	30m	GAIA	“Exclusion/Inclusion” approach	(Gong et al., 2020)

410

https://doi.org/10.5194/essd-2020-107
Preprint. Discussion started: 25 June 2020

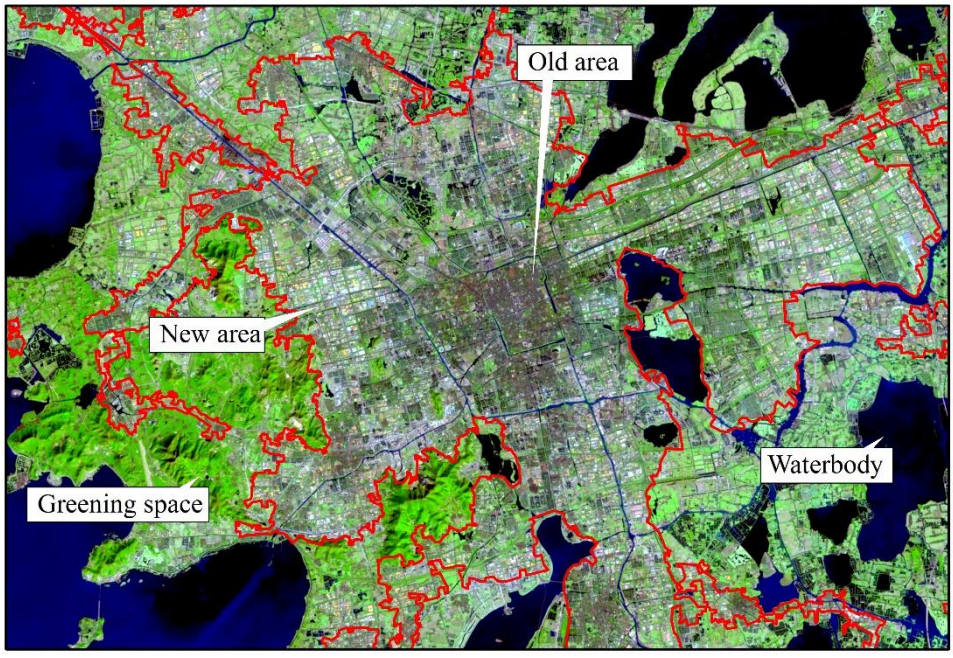

Figure 1: Landsat image and digital urban boundary (in red) of Suzhou, China (December 29, 2014, Landsat 8 OLI, composite of Shortwave Infrared, Near-Infrared and Red bands). (The Landsat image is provided by Geospatial Data Cloud site, Computer Network Information Center, Chinese Academy of Sciences (http://www.gscloud.cn))

https://doi.org/10.5194/essd-2020-107
Preprint. Discussion started: 25 June 2020

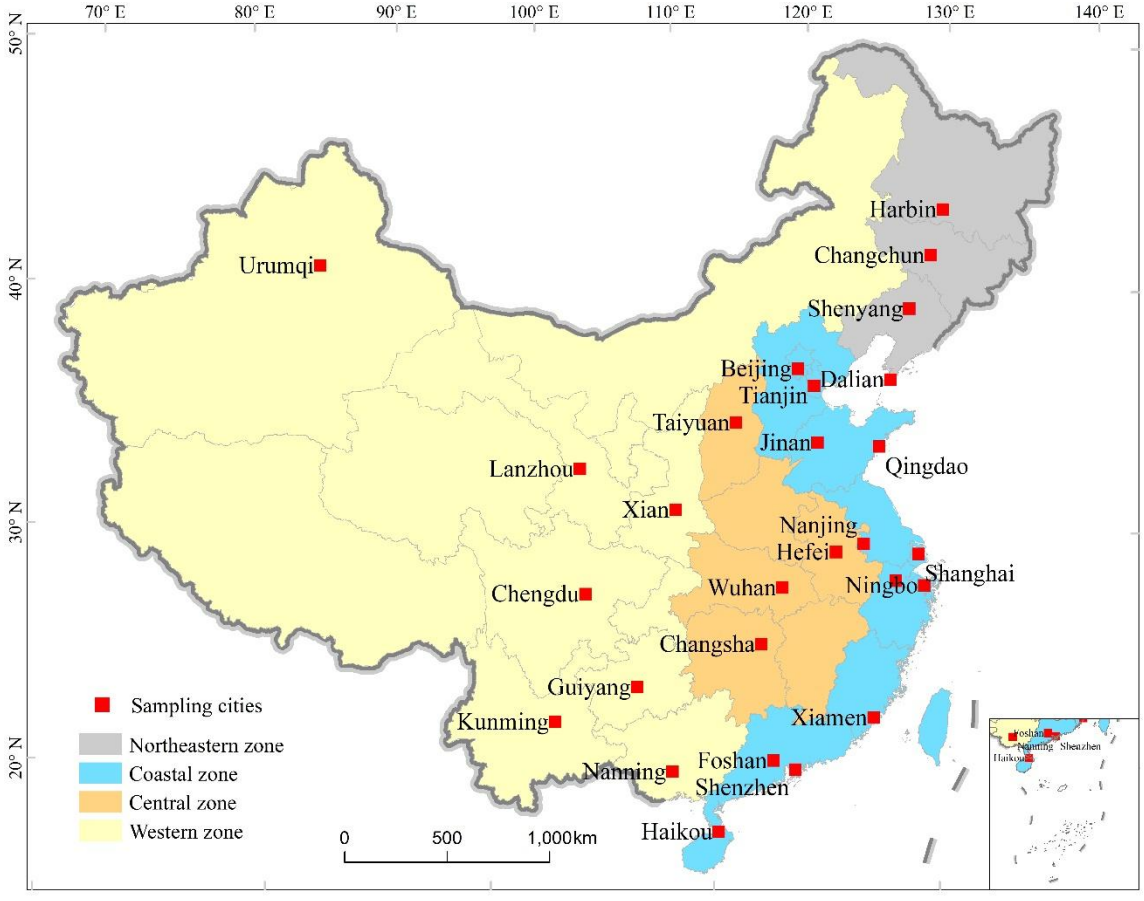

Figure 2: **Spatial distribution of 28 sample cities located in different regions of China. (The administrative boundaries were provided by National Geomatics Center of China (http://www.webmap.cn))**

https://doi.org/10.5194/essd-2020-107
Preprint. Discussion started: 25 June 2020

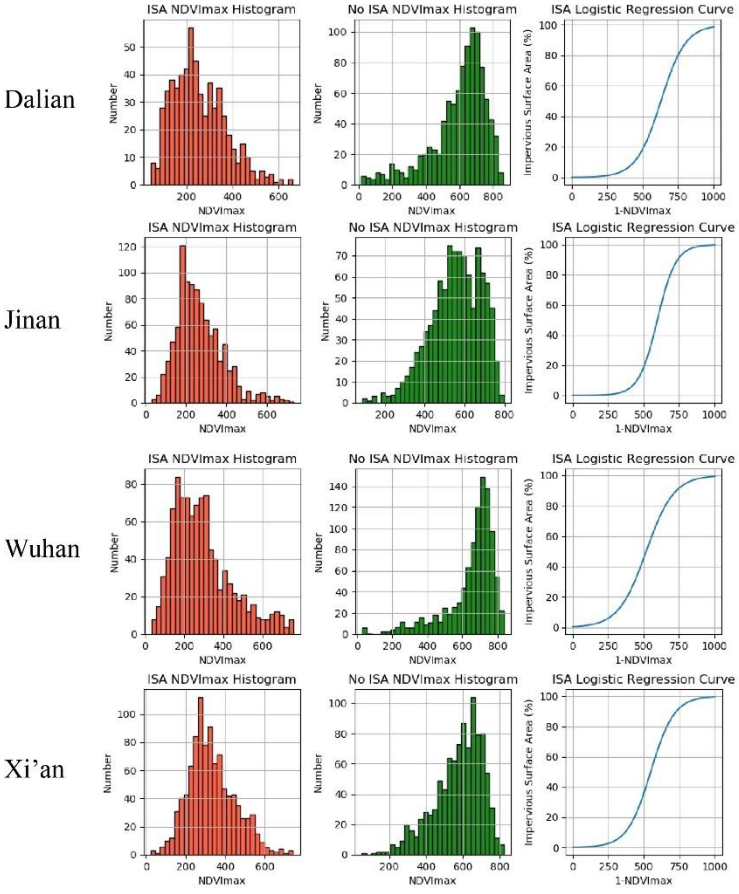

420 **Figure 3**: **Relationships between UISAs and annual NDVI maximum values in four sample cities in China.**

https://doi.org/10.5194/essd-2020-107
Preprint. Discussion started: 25 June 2020

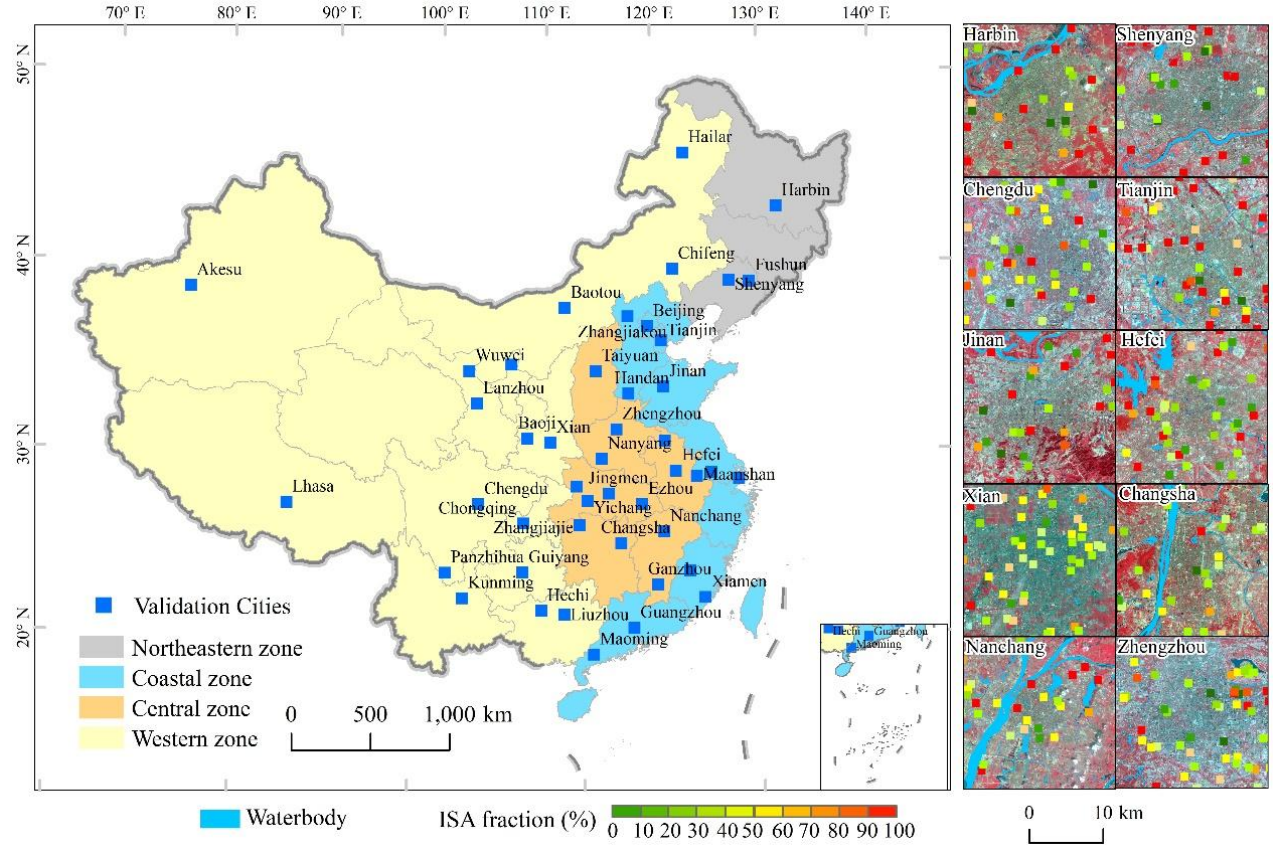

Figure 4: Distribution of 44 validation cities and points in China. (The image is provided by Geospatial Data Cloud site, Computer Network Information Center, Chinese Academy of Sciences (http://www.gscloud.cn). The administrative boundaries were provided by National Geomatics Center of China (http://www.webmap.cn))

https://doi.org/10.5194/essd-2020-107
Preprint. Discussion started: 25 June 2020

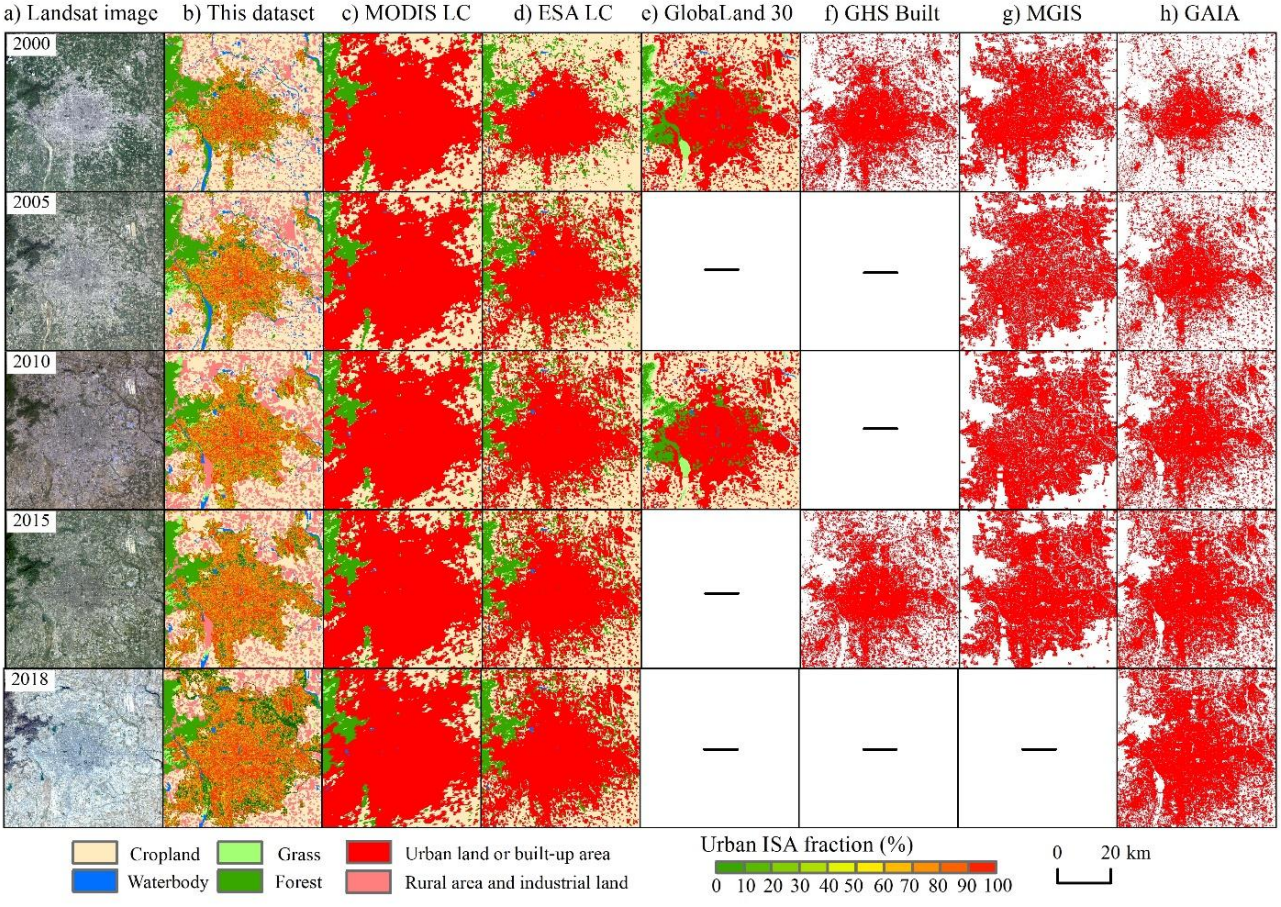

425

Figure 5: A comparison of urban land classification results in Beijing among different urban land products (The Landsat image is provided by Geospatial Data Cloud site, Computer Network Information Center, Chinese Academy of Sciences (http://www.gscloud.cn))

430

https://doi.org/10.5194/essd-2020-107
Preprint. Discussion started: 25 June 2020

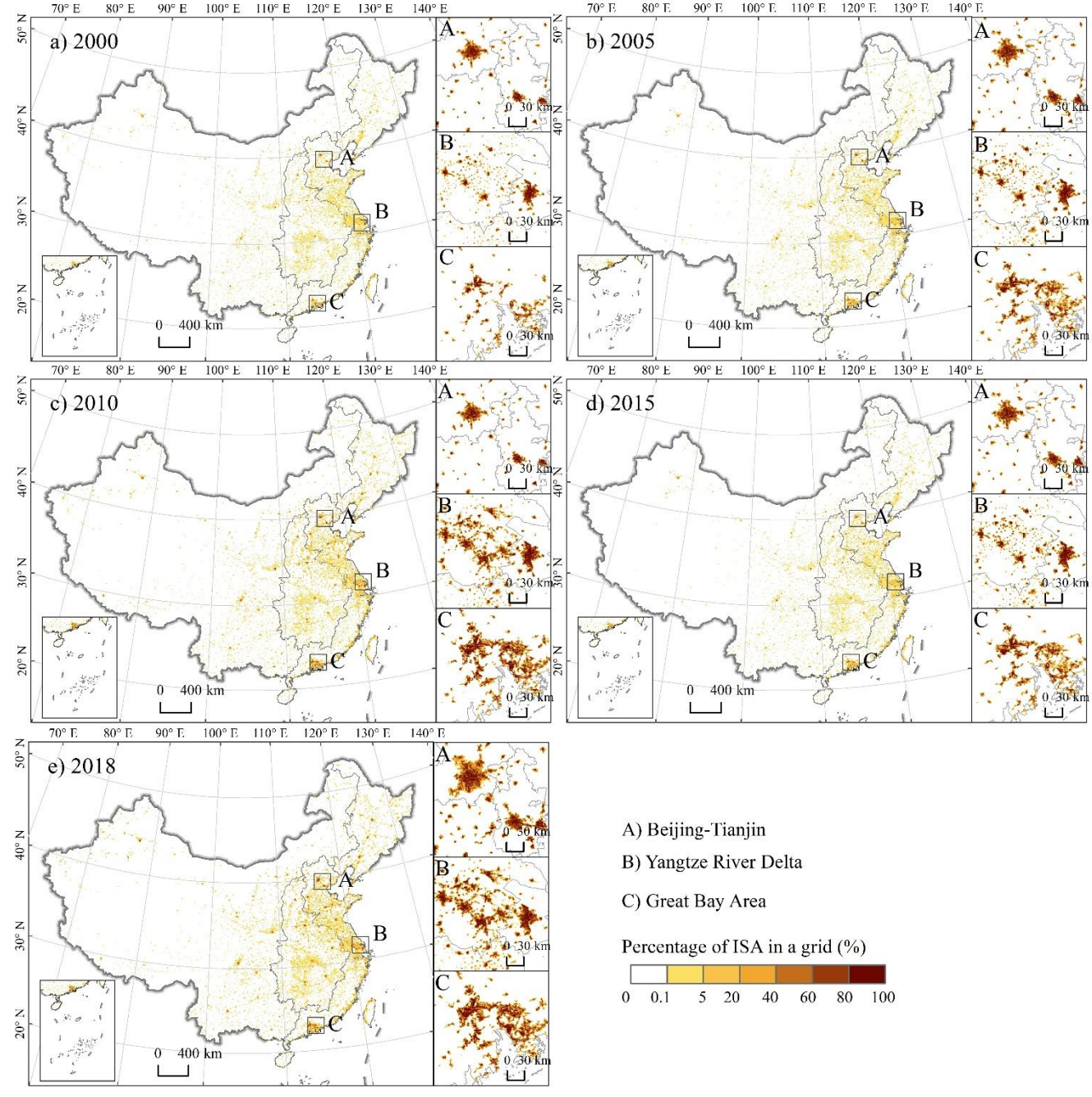

Figure 6: Spatial distribution of impervious surface area (ISA) in China, 2000–2018, at five-year intervals. (The administrative boundaries were provided by National Geomatics Center of China (http://www.webmap.cn))

https://doi.org/10.5194/essd-2020-107
Preprint. Discussion started: 25 June 2020

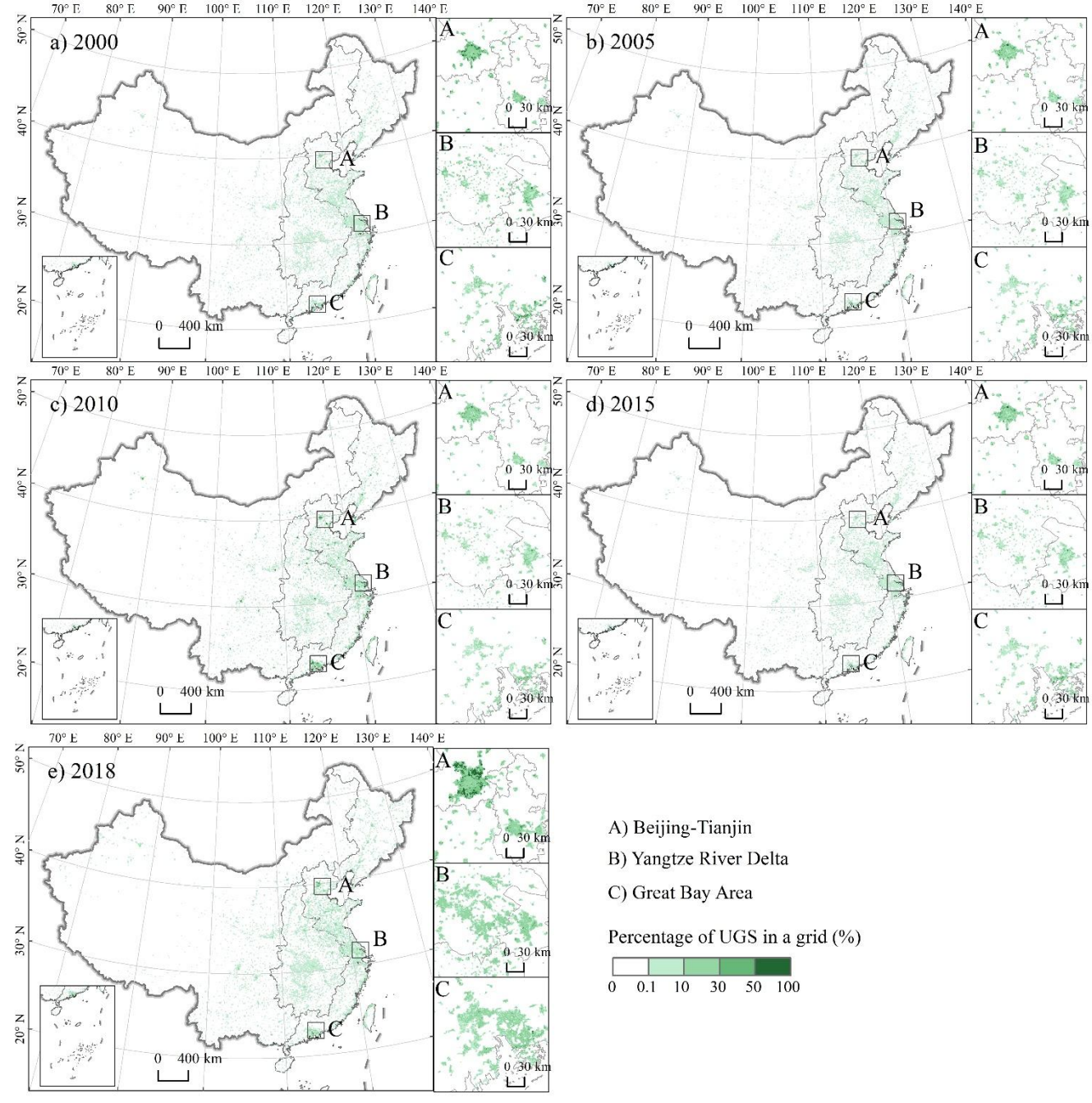

435 **Figure 7: Spatial distribution of urban green space (UGS) in China, 2000–2018 at five-year intervals. (The administrative boundaries were provided by National Geomatics Center of China (http://www.webmap.cn))**

https://doi.org/10.5194/essd-2020-107
Preprint. Discussion started: 25 June 2020

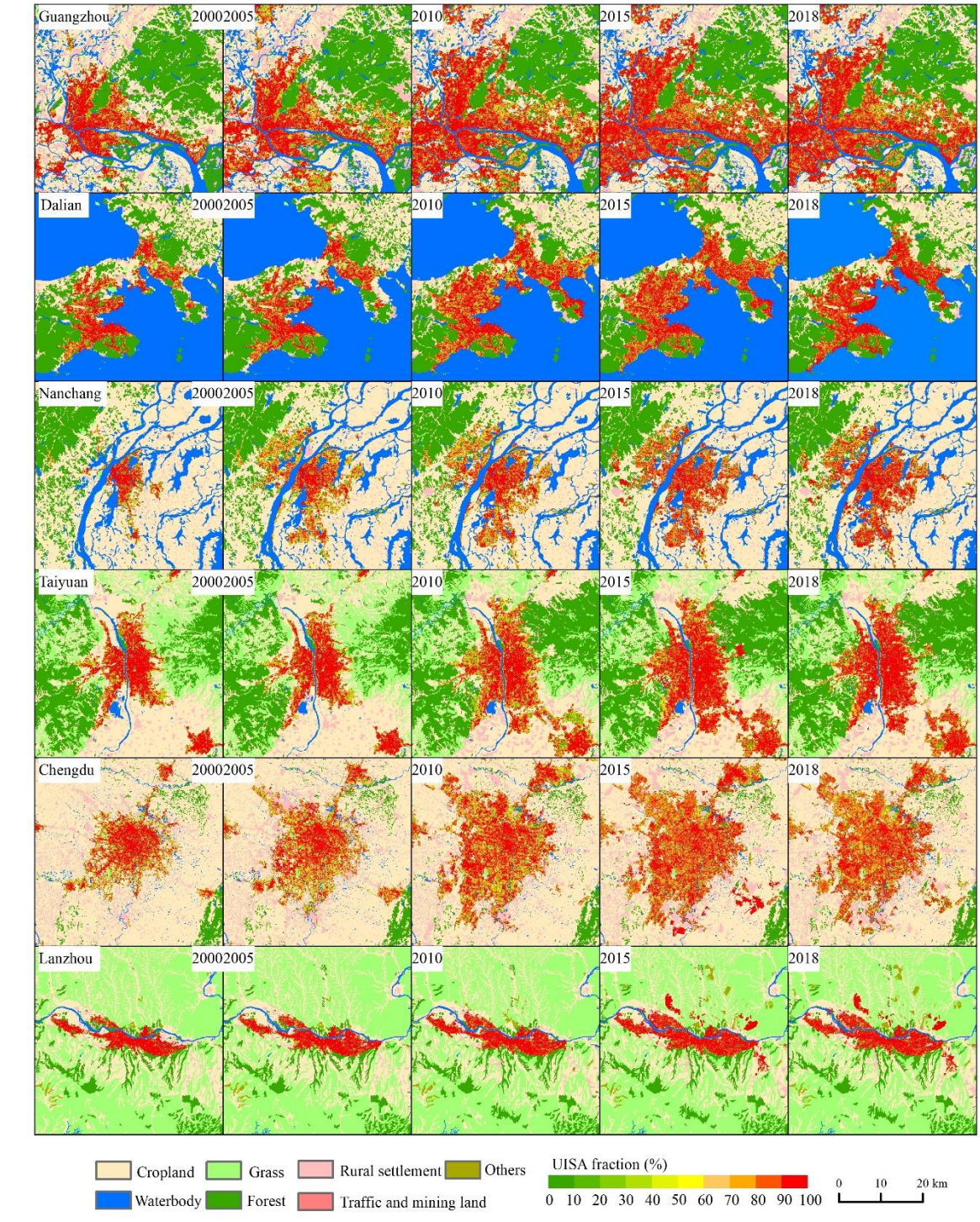

Figure 8: A comparison of urban land cover fractions among typical cities in China.